Supporting Information

Reprocessing of cross-linked polyamide networks via catalyst-free methods under moderate conditions

Jinshuai Zhang [a, b], Yonghong Zhou [b*], Shuanhong Ma [a, c*], Feng Zhou [c]

[a] Shandong Laboratory of Advanced Materials and Green Manufacturing at Yantai, Yantai Zhongke Research Institute of Advanced Materials and Green Chemical Engineering, Yantai 264006, China

[b] Institute of Chemical Industry of Forest Products, Chinese Academy of Forestry, Nanjing 210042, China

[c] State Key Laboratory of Solid Lubrication, Lanzhou Institute of Chemical Physics, Chinese Academy of Sciences, Lanzhou 730000, China

Corresponding authors

[*] E-mail addresses: zyh@icifp.cn (Y. Zhou); mashuanhong@licp.cas.cn (S. Ma).

Table of Contents

1. Materials and Characterizations

1.1. Materials

Tung oil (TO) was provided by Jiangsu Donghu Bioenergy Plant Plantation Co., Ltd. (Yancheng, China). Hexahydrophthalic anhydride, (HHPA, 98%), N-*tert*-butylmethylamine (TBMA, 95%), N-isopropylmethylamine (IPMA, 98%), N-ethylmethylamine (EMA, 98%), phthalic anhydride (PA, 99.5%), cyclohexanecarbonyl chloride (CHCC, 98%), cyclohexanecarboxylic acid (99.5%), 2-(*tert*-butylamino)ethyl methacrylate (TBEM, >98%), trimethylamine (99%), maleic anhydride (MA, 99%), 2-hydroxyethyl acrylate (HEA, 97%), dimethyl sulfoxide-d6 (DMSO-d6, 99.9%), tetrahydrofuran (THF, 99.9%), dichloromethane (99%), ethanol (99.7%), and Darocur 1173 (97%) were purchased from Maclin Chemical Reagent Co., Ltd. Magnesium sulfate ($MgSO_4$, 98%) was purchased from Sinopharm Chemical Reagent Co., Ltd. (China). All the reagents and solvents in the study were used without further purification.

1.2. Characterizations

Fourier transform infrared (FT-IR) analyses were conducted using a Nicolet iS10 IR spectrometer (Nicolet Corporation, USA), covering a scan range of 4000 to 550 cm^{-1}. Temperature-dependent FT-IR spectra were obtained by applying a thin film onto a NaCl crystal. Typically, the time elapsed between mixing and the initial spectrum collection was less than 5 min. Following the initial calibration of the FT-IR spectra, the temperature was gradually elevated from 20 ^oC to 80 ^oC (or 100 ^oC/ 200 ^oC), in 10 ^oC increments, with a 5-min equilibration period at each temperature. Nuclear magnetic resonance (NMR) tests were conducted on a DRX-300 Advance NMR spectrometer (Bruker Corporation, Germany). Deuterated chloroform or dimethyl sulfoxide-d6 was used as solvent. Electrospray ionization mass spectrometry (ESI-MS) was recorded on a Thermo-QE plus (USA) apparatus. Relative molecular weights: To test the samples, a high-performance liquid chromatography (HPLC) device was utilized, which consisted of Styragel HR1 and HR2 (300 mm × 7.8 mm) columns connected to a 2414 refractive index detector (Waters Corporation, USA). The columns were maintained at a temperature of 35 ^oC, and THF was used as the solvent with a flow rate of 1.0 mL/min. Sample solutions were prepared using THF as a solvent and collected with a concentration of 10-20 mg/mL. The relative molecular weights of the samples were determined using a calibration curve generated from polystyrene standards with molecular weights ranging from 580 to 19,600. Gel content

(C_{gel}) of the prepared samples was measured using Soxhlet extraction, as described in our previous work [1]. UV-curing kinetics were evaluated by tracing the intensity of the peak at 810 cm^{-1} using a modified Nicolet 5700 spectrometer (Thermo-Nicolet Corporation, USA). Dynamic mechanical analysis (DMA) was conducted using a Q800 solids analyzer (TA Corporation, USA) over a temperature range of -60 °C to 180 °C, with a heating rate of 3 °C/ min and a frequency of 1 Hz. The glass transition temperature (T_g) was determined from the peak temperature of the tan δ curves, while the crosslink density (v_e) was calculated using the following equation [2, 3]:

$$v_e = \frac{E'}{3RT} \quad \text{(Eqn. S1)}$$

where E' is the storage modulus in the rubber state (T_g + 50 °C was adopted in this work), R is the gas constant, and T is the absolute temperature. Thermogravimetric analysis (TGA) was conducted using an STA 409PC thermogravimetry instrument (Netzsch Corporation, Germany) over a temperature range of 40 °C to 600 °C, with a heating rate of 10 °C/ min under a nitrogen atmosphere. Differential scanning calorimetry (DSC) measurements were performed on a DSC8000 calorimeter (PerkinElmer Corporation, USA) within the temperature range of -60 °C to 180 °C, with a heating rate of 20 °C/min under a nitrogen atmosphere. To eliminate the thermal history, the second scan was utilized to determine the T_g values of the UV-cured materials. The tensile properties of the samples were measured using a UTM 4304 universal tester (Shenzhen Suns Technology Corporation, China) with a cross-head speed of 10 mm/min. For each sample, five specimens were tested to calculate the average values. The stress relaxation curves of the samples were obtained using a DMA Q800 instrument, applying a strain value of 5% in “stress relaxation” mode. Rheological measurements of the samples were performed using a HAAKE MARS II rheometer (Germany) with a 25 mm parallel plate set-up. The measurements were conducted with a fixed gap of 1.5 mm and a deformation of 1%, which fell within the linear viscoelastic region. The scratch-repairing processes of the films were investigated through the monitoring of scratch recovery using a Leica optical microscope (Germany, ICC50 W). The film was scratched to have a crack on the surface by using a razor blade, and the width of the crack was measured by using a microscope. Subsequently, the film was subjected to heating in an oven at temperatures of 80 °C, 100 °C, 140 °C, and 180 °C for various time intervals under pressure-free conditions. The self-healing efficiency was calculated by dividing the reduced scratch width by the initial scratch width of the materials. Extrusion tests were performed using a HAAKE Minilab II

micromixed extruder (Germany). The extrusion conditions were set as follows: temperature of 140 °C, time of 30 min, torque of 550 N·cm, and rotational speed of 60 rpm.

2. Synthesis of low-molecular-weight (LMW) model compounds

The synthesis of LMW model compounds, namely compounds **5**, **6**, and **7** (**Scheme S1**), was conducted using the same procedure as compound **1**. To synthesize compound **4**, 0.91 g (10.0 mmol) of TBMA was combined with 50 mL of dry dichloromethane along with 1.2 g (12.0 mmol, 1.2 eq) of trimethylamine. The mixture was placed under a nitrogen atmosphere and cooled using an ice bath. Then, 1.80 g (12.0 mmol, 1.2 eq) of CHCC was slowly added dropwise to the solution. After stirring at room temperature for 5 h, the mixture was cooled again to 0 °C, and 25 mL of water was added to quench the excess CHCC. Following an additional 30 min of stirring, the organic layer was separated using a separating funnel and washed three times with saturated $NaHCO_3$ solution and with distilled water until neutral. It was then dried with $MgSO_4$ and subjected to rotary evaporation to remove the dichloromethane. Finally, a transparent liquid product was obtained, yielding 1.66 g (84.2%).

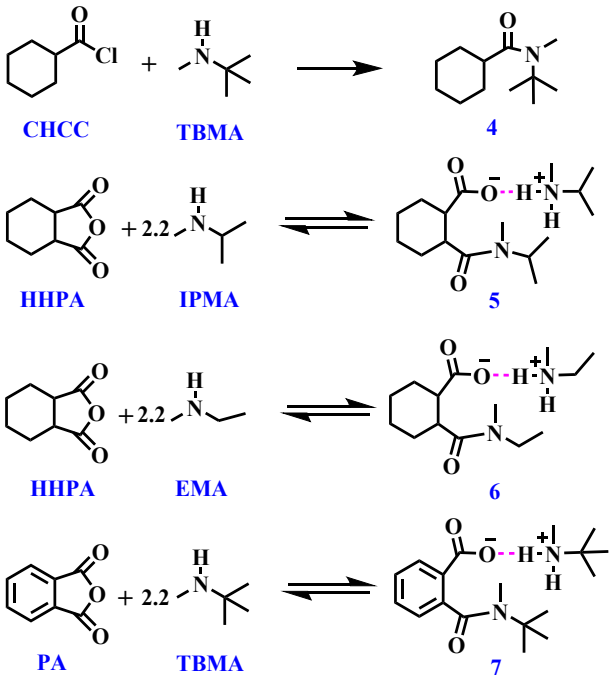

Scheme S1. Synthesis routes of LMW model compounds **4**-**7**.

3. Supplement Figures and Tables

3.1. FT-IR spectrum, ^{1}H NMR spectrum, and ESI-MS spectrum of compound 1

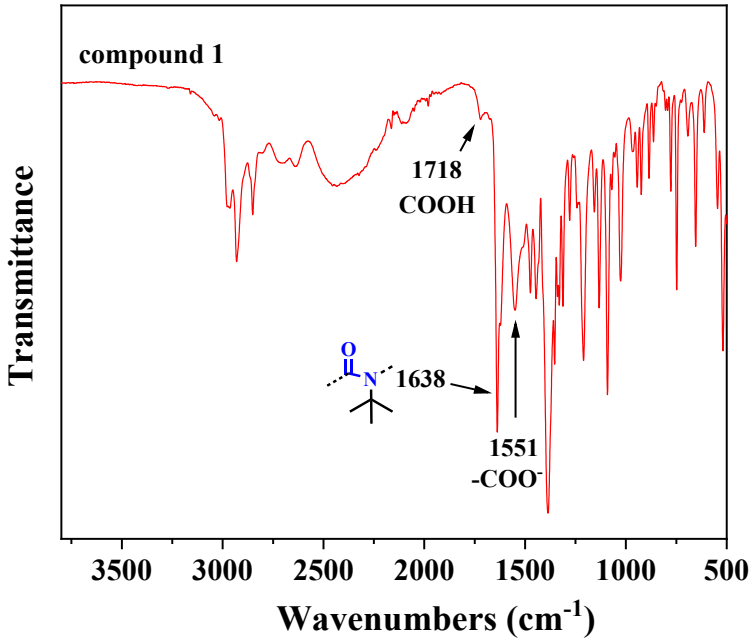

Fig. S1. FT-IR spectrum of compound **1** (TBMA/HHPA ratio 2.2).

In the FT-IR spectrum of compound **1**, a prominent amide bond (-N-CO-) peak is evident at 1638 cm^{-1}, while the carboxylate ion peak is observed at 1551 cm^{-1}. [4, 5] It is worth noting that there are no characteristic peaks of acid anhydrides around 1860 and 1780 cm^{-1}, indicating complete ring-opening reactions of the acid anhydride moiety. [1]

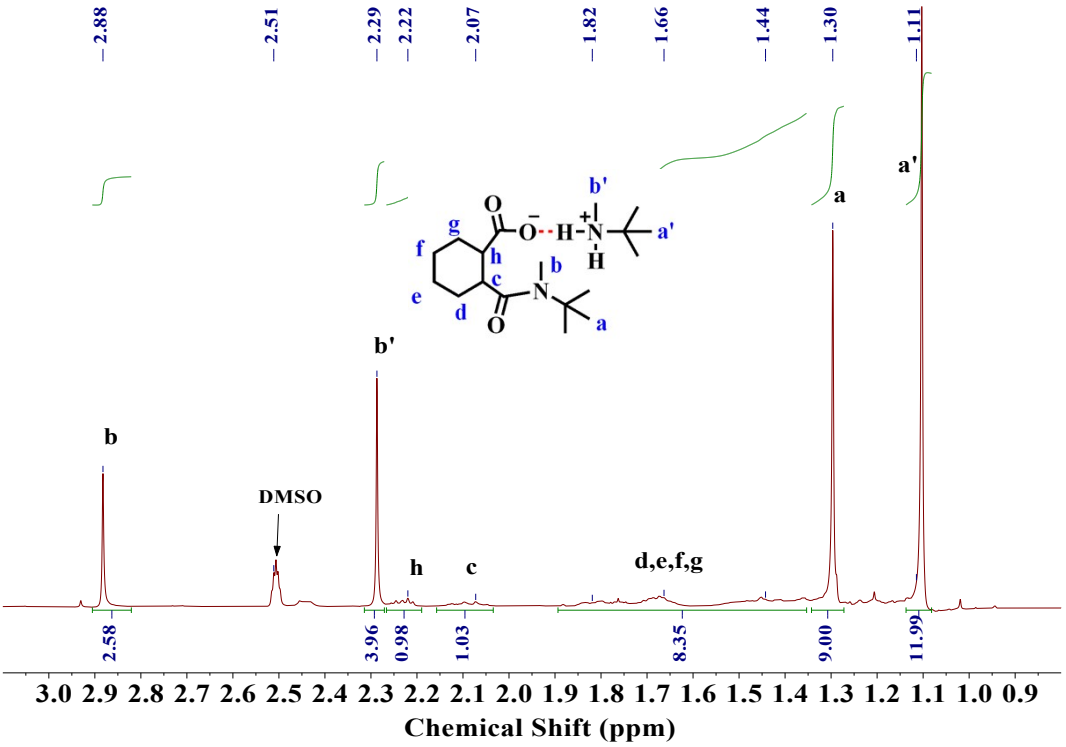

Fig. S2. ^{1}H NMR spectrum of compound **1** (TBMA/HHPA ratio 2.2).

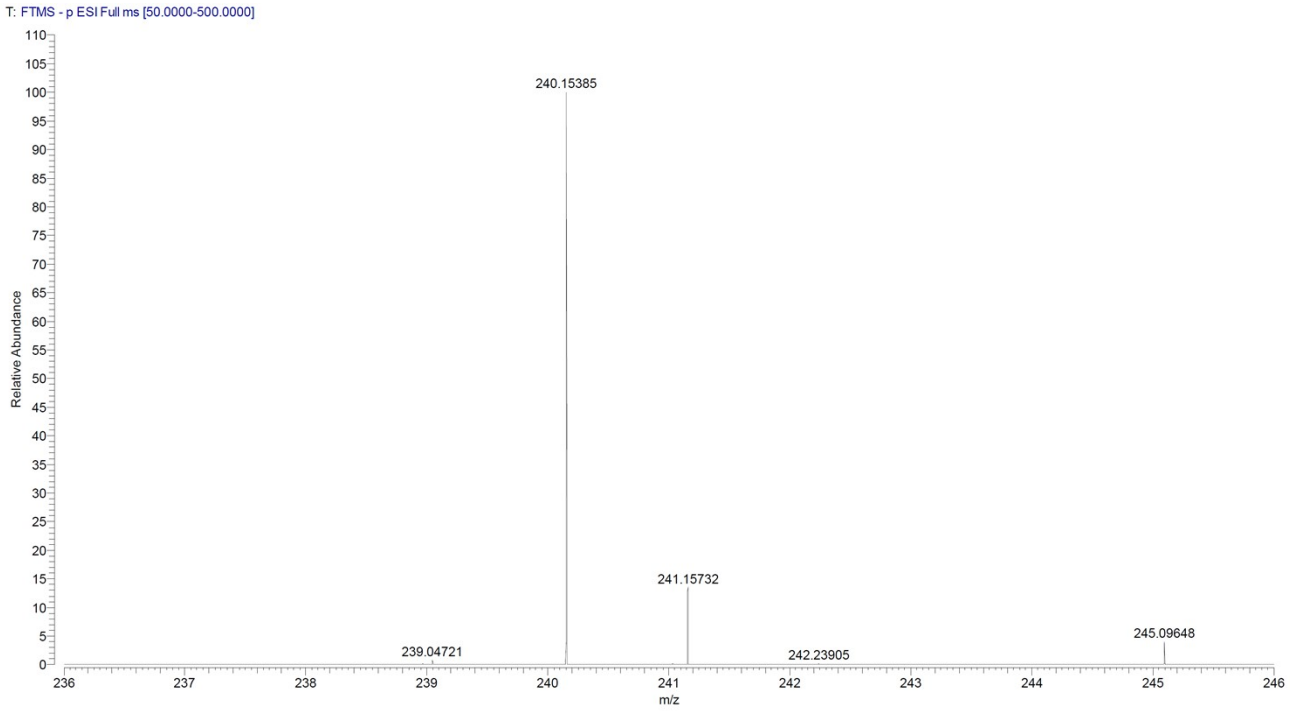

Fig. S3. ESI-MS spectrum of compound **1**. The mass peak with a found m/z for $[M-H]^-$ is close to its calculated m/z of 240.32.

3.2. FT-IR spectrum, ^{1}H NMR spectrum, and ESI-MS spectrum of compound 5

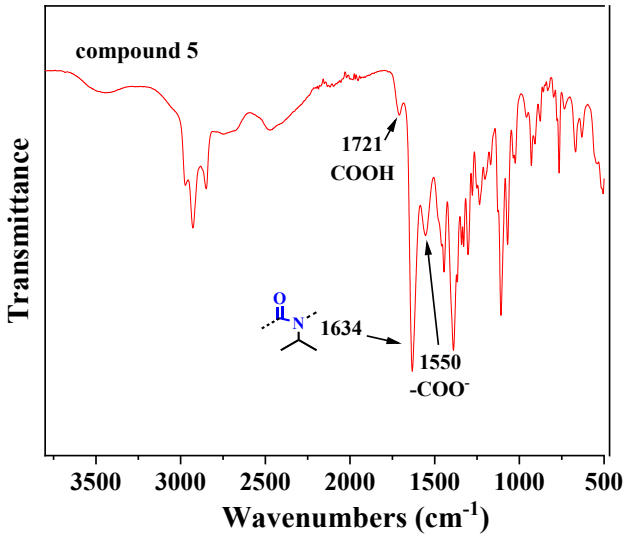

Fig. S4. FT-IR spectrum of compound **5** (IPMA/HHPA ratio 2.2).

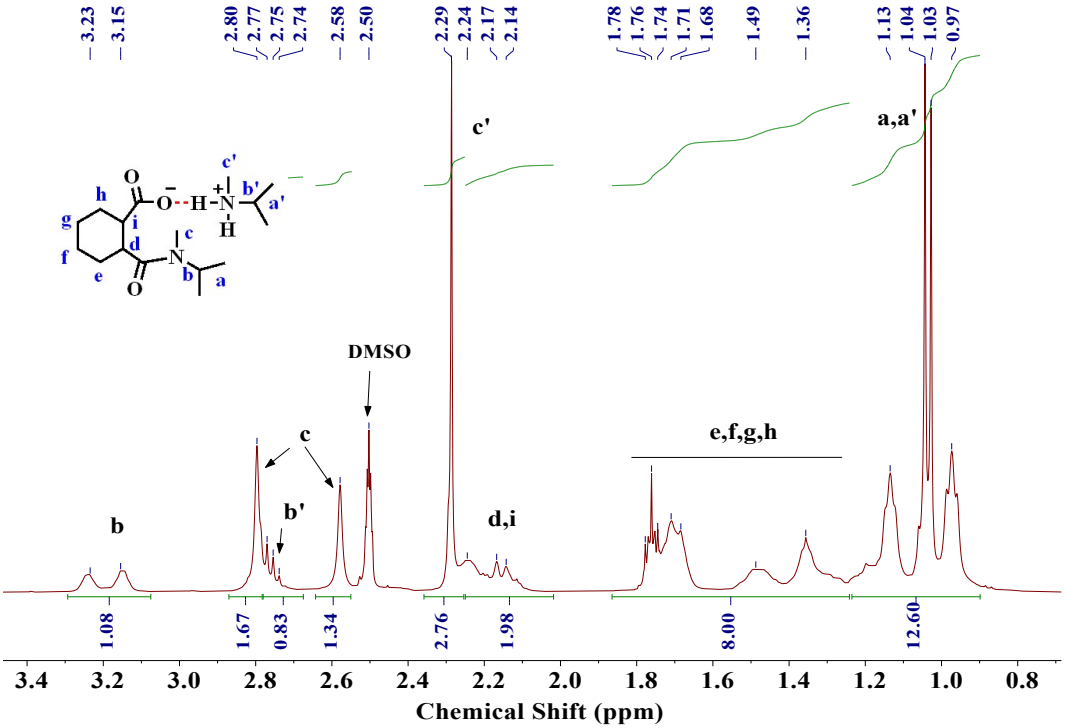

Fig. S5. ^{1}H NMR spectrum of compound **5** (IPMA/HHPA ratio 2.2).

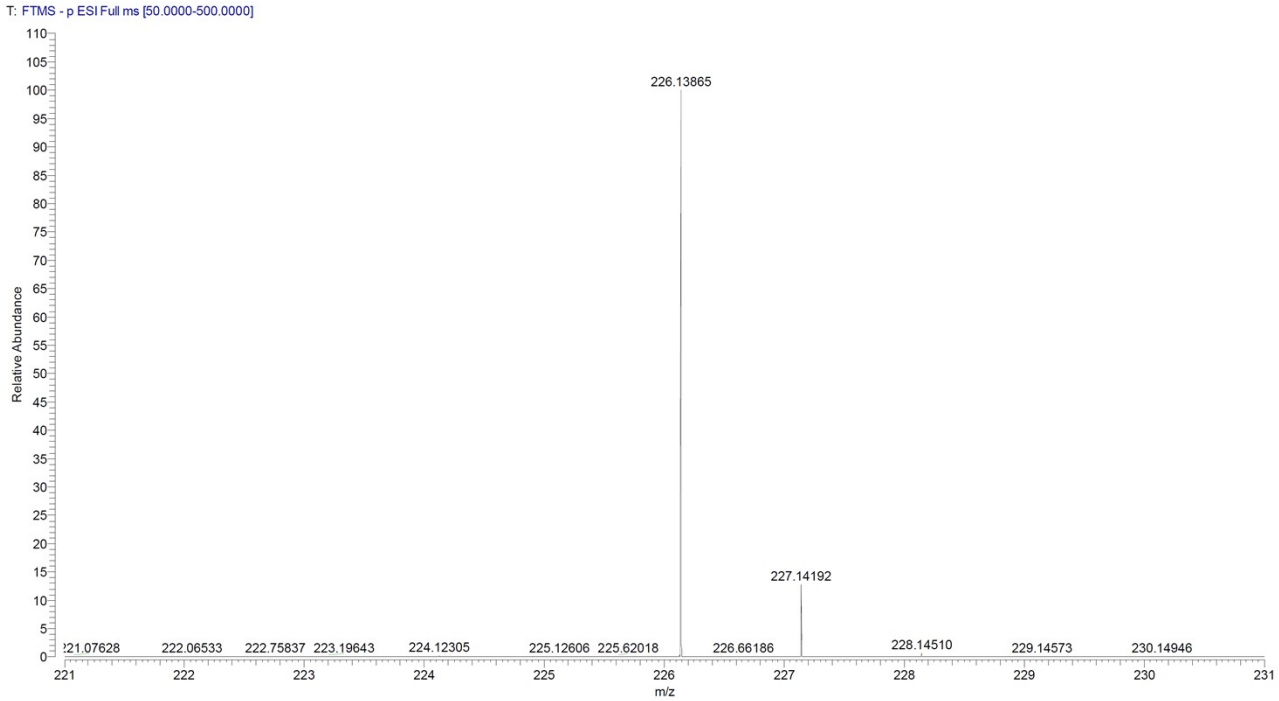

Fig. S6. ESI-MS spectrum of compound **5**. The mass peak with a found m/z for $[M-H]^-$ is close to its calculated m/z of 226.40.

3.3. FT-IR spectrum, ^{1}H NMR spectrum, and ESI-MS spectrum of compound 6

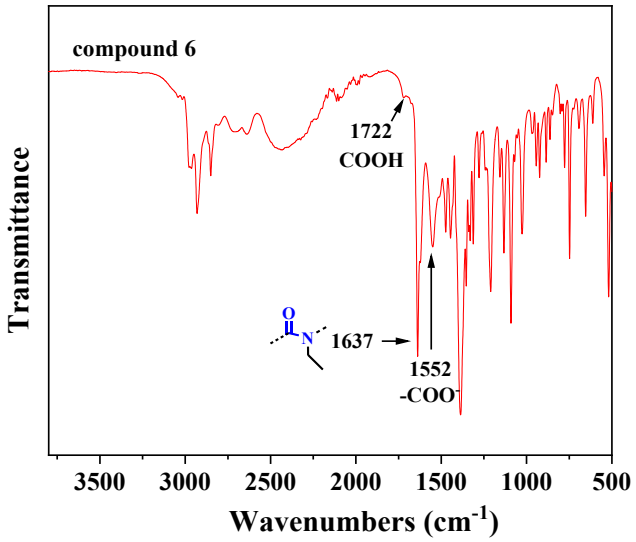

Fig. S7. FT-IR spectrum of compound **6** (EMA/HHPA ratio 2.2).

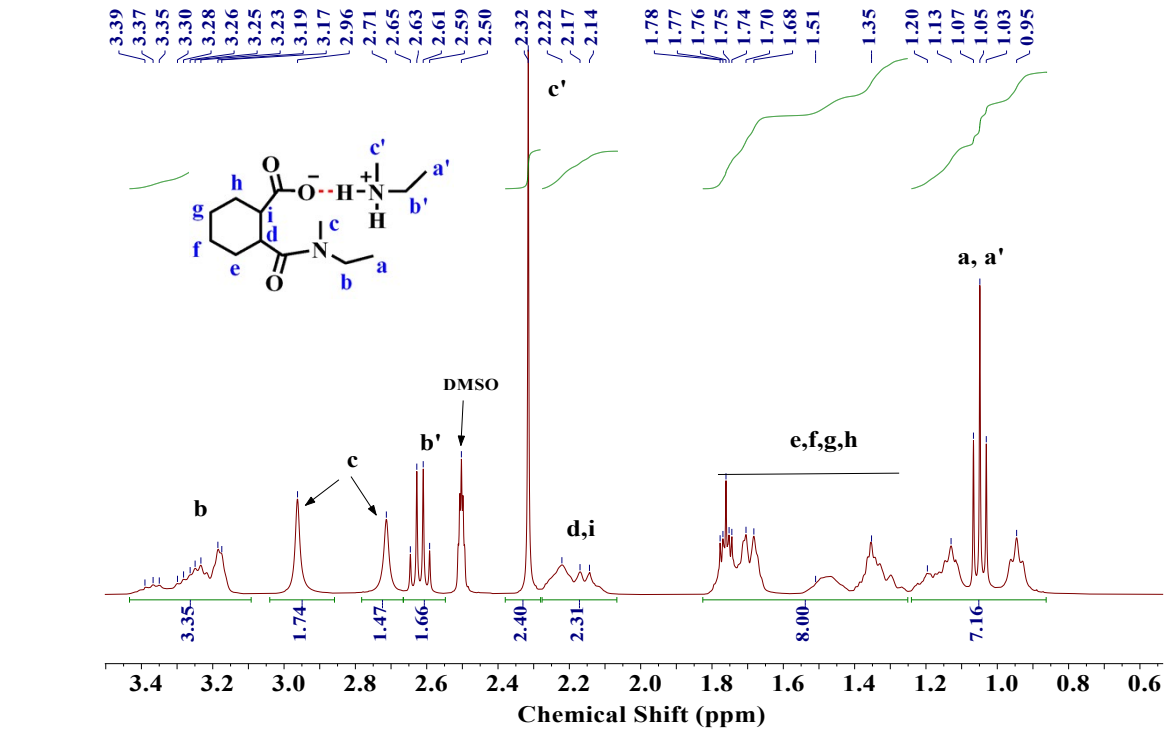

Fig. S8. ^{1}H NMR spectrum of compound **6** (EMA/HHPA ratio 2.2).

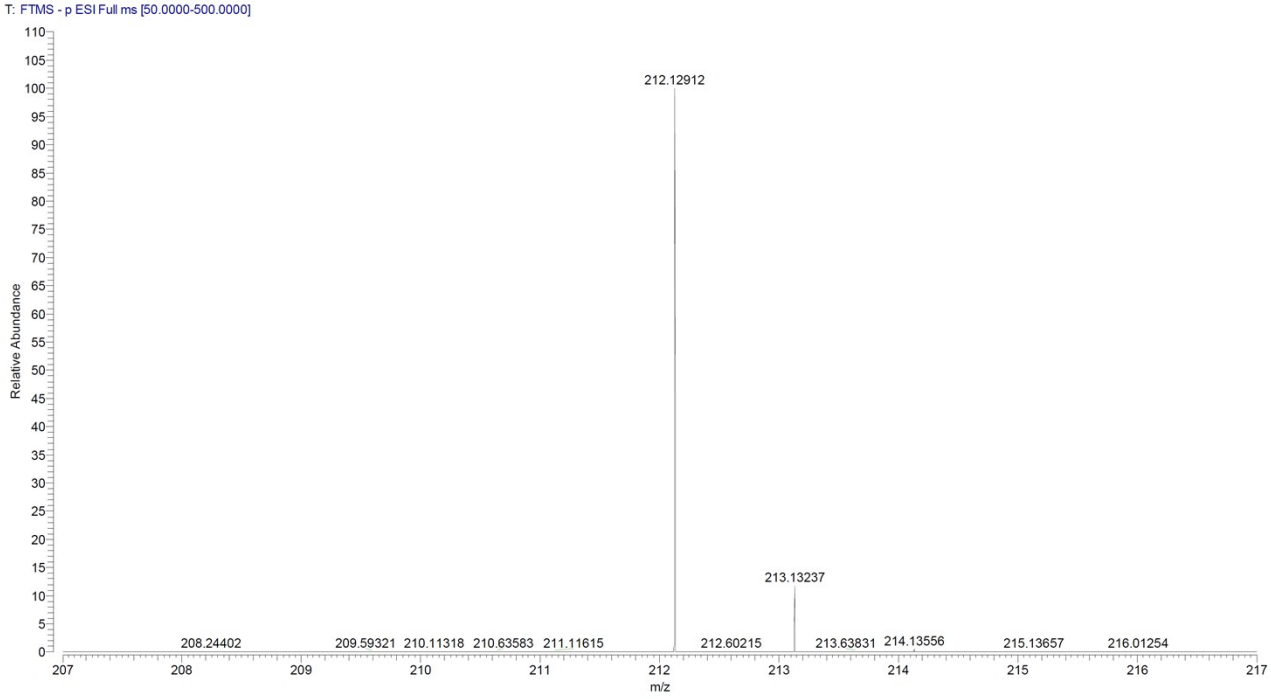

Fig. S9. ESI-MS spectrum of compound **6**. The mass peak with a found m/z for $[M-H]^-$ is close to its calculated m/z of 212.27.

3.4. FT-IR spectrum and ^{1}H NMR spectrum of compound 4

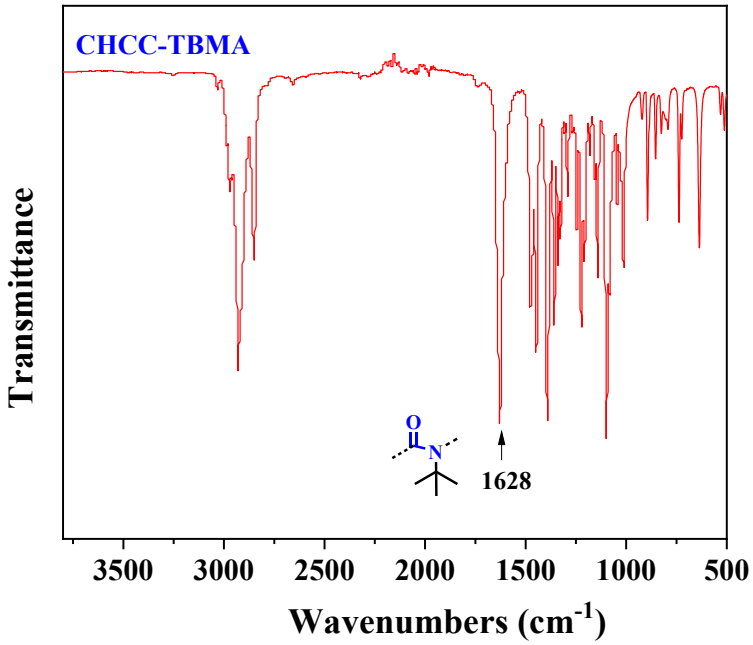

Fig. S10. FT-IR spectrum of compound **4**.

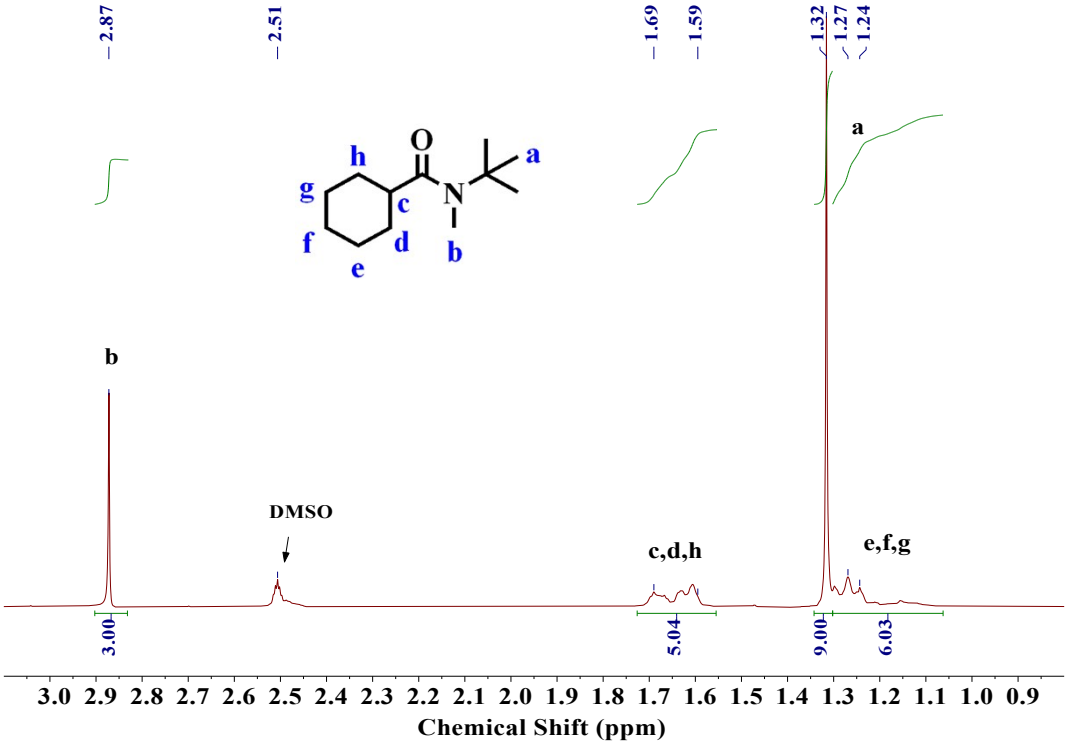

Fig. S11. ^{1}H NMR spectrum of compound **4**.

3.5. FT-IR spectrum and ^{1}H NMR spectrum of compound 7

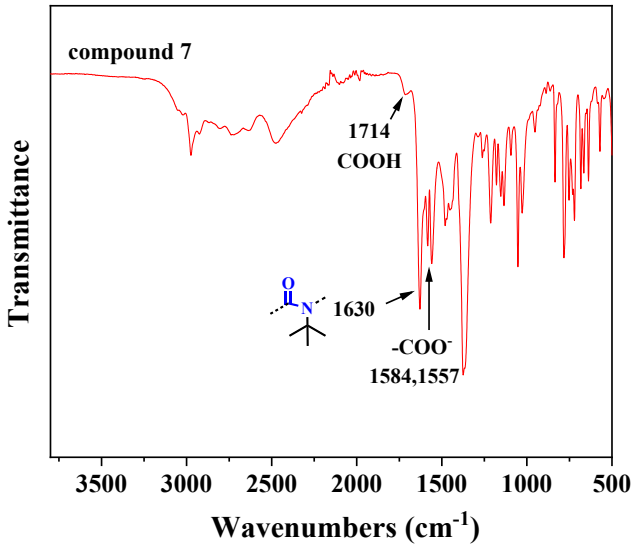

Fig. S12. FT-IR spectrum of compound **7** (TBMA/PA ratio 2.2).

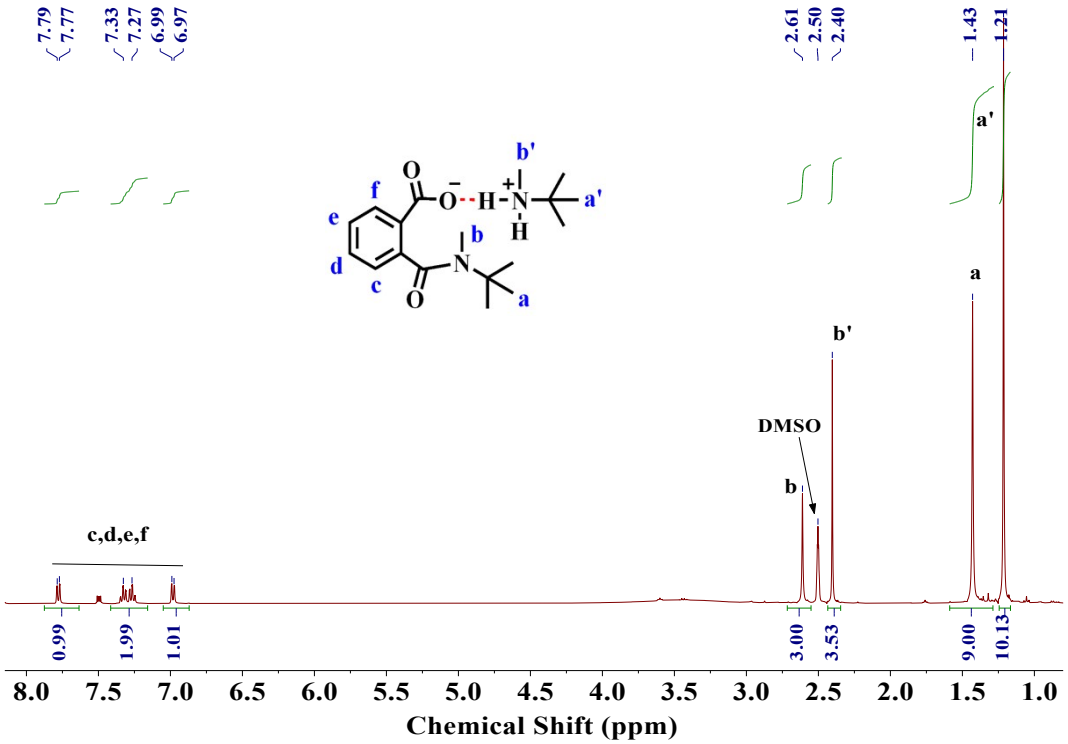

Fig. S13. ^{1}H NMR spectrum of compound **7** (TBMA/PA ratio 2.2).

3.6. ^{1}H NMR spectra of compound 4 before and after heating

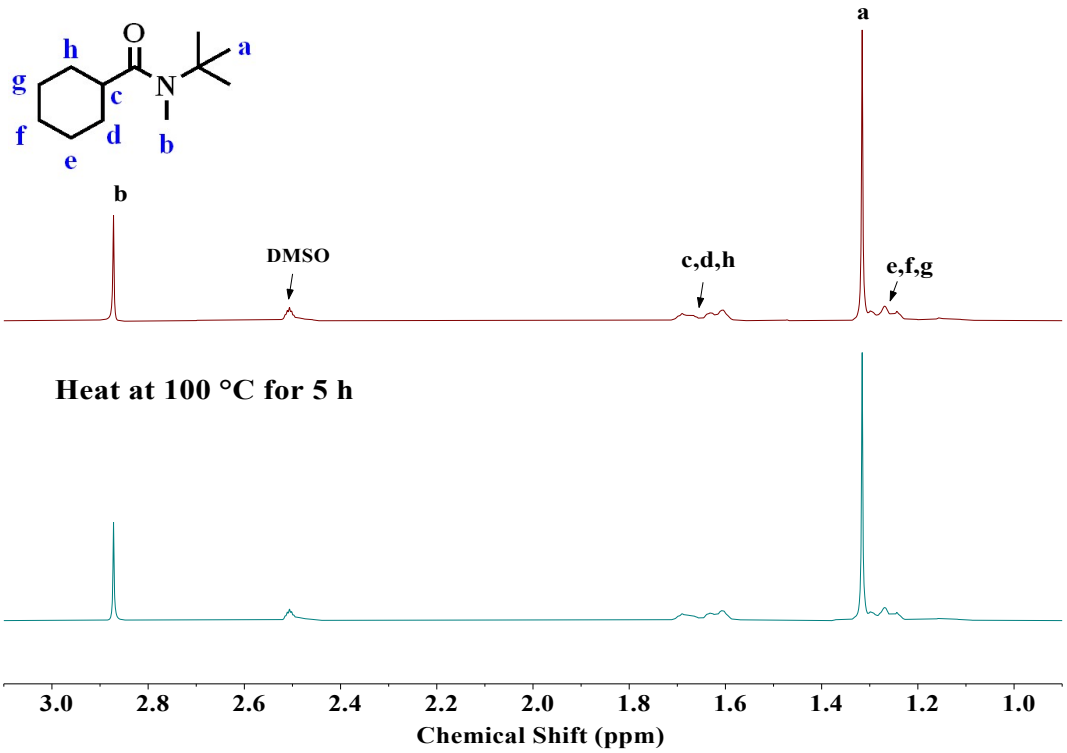

Fig. S14. ^{1}H NMR spectra of compound **4** before and after heating.

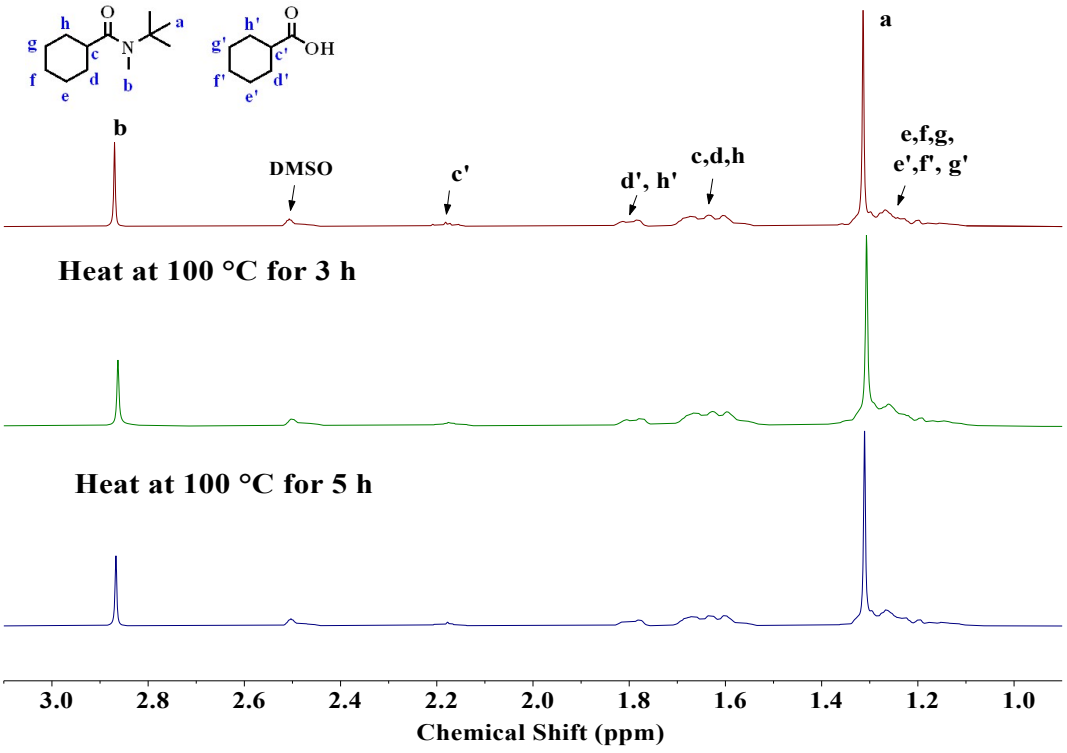

Fig. S15. ^{1}H NMR spectra of compound **4** + cyclohexanecarboxylic acid before and after heating.

3.7. Temperature-dependent FT-IR spectra of compound 7

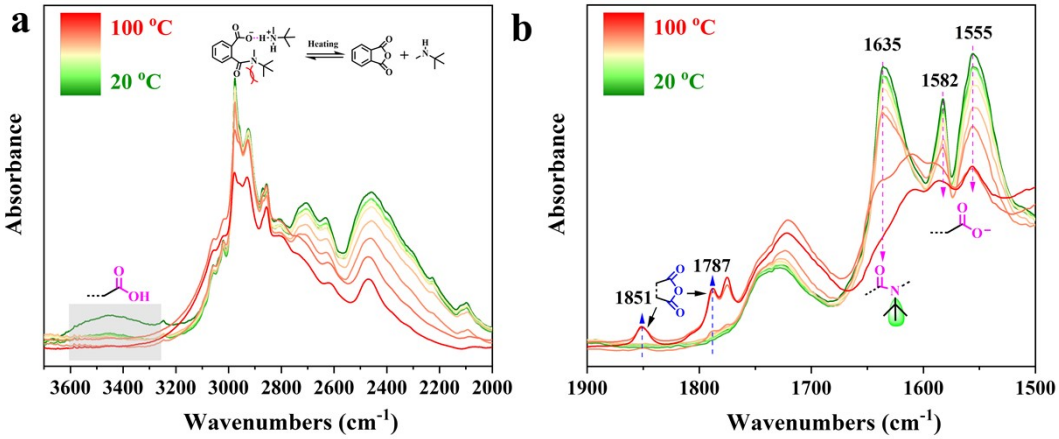

Fig. S16. Temperature-dependent FT-IR spectra of compound **7**.

3.8. FT-IR spectra, ^{1}H NMR spectra, and GPC spectra of the TO, TOMA, and TMH

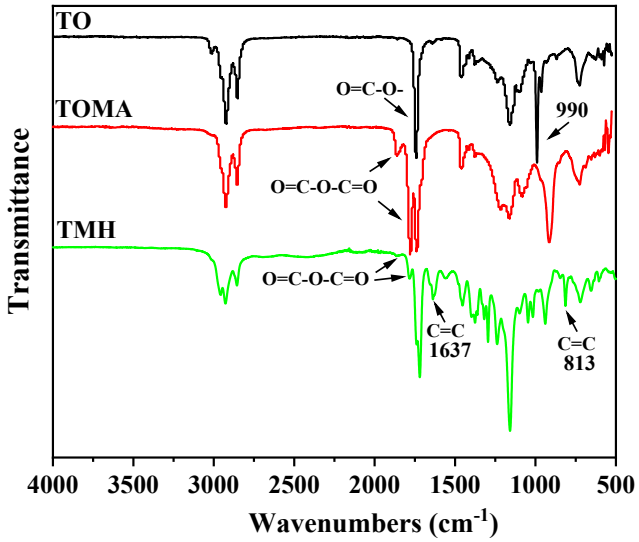

Fig. S17. FT-IR spectra of TO, TOMA, and TMH.

In the TO spectrum, the strong absorption bands at 1742 and 990 cm^{-1} were assigned to the characteristic peaks of ester C=O stretching vibration and conjugated triene C=C vibration, respectively. In the TOMA spectrum, new peaks emerged at 1843 and 1778 cm^{-1}, corresponding to the asymmetric stretching vibration of the O=C-O-C=O anhydride group. Additionally, the C=C absorption peak at 990 cm^{-1} disappeared, indicating the occurrence of a reaction between TO-conjugated trienes and MA. In the TMH spectrum, the intensities of the peaks at 1843 and 1778 cm^{-1}, corresponding to the anhydride group, significantly decreased compared to the ester peak at around 1742 cm^{-1}. New peaks appeared at 1637 and 813 cm^{-1}, corresponding to C=C stretching and bending vibrations, respectively.

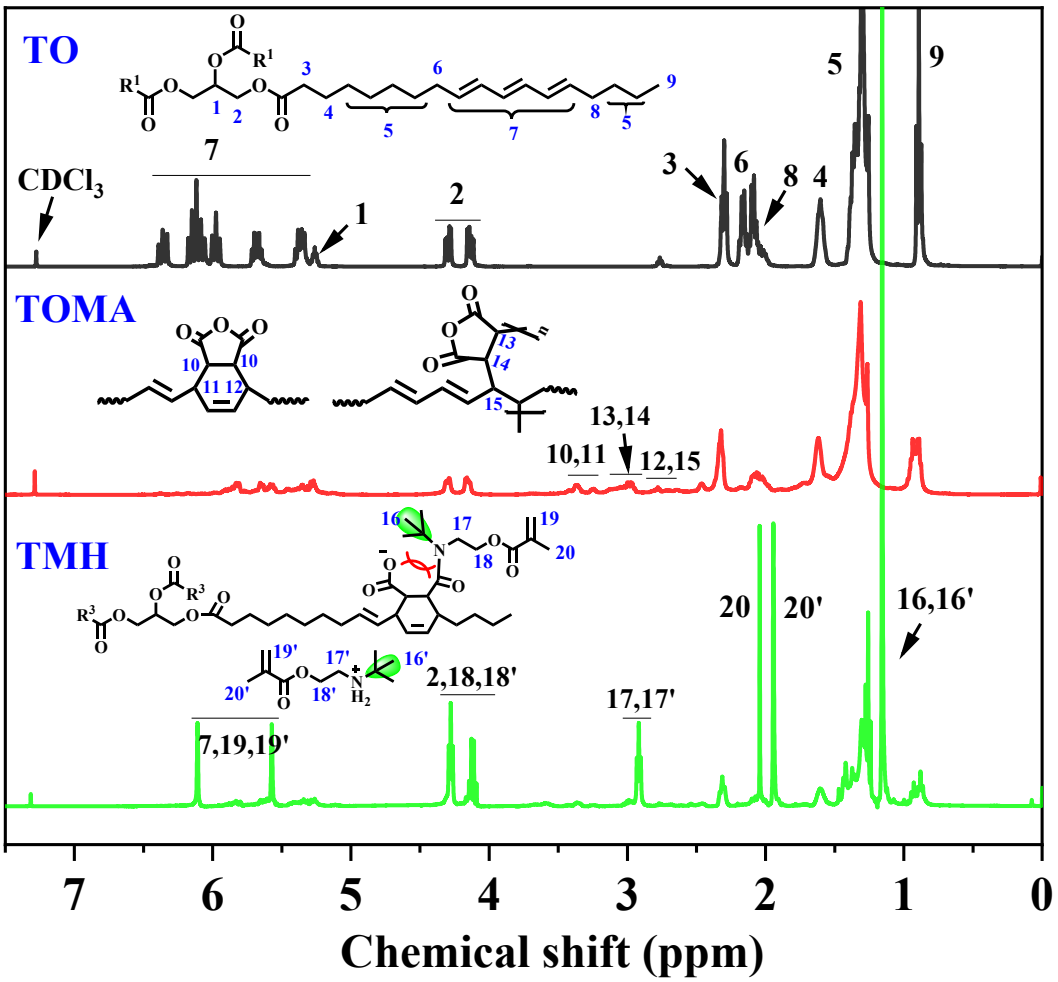

Fig. S18. ^{1}H NMR spectra of TO, TOMA, and TMH.

In the TO spectrum, the multiple peaks in the range of 5.3-6.5 ppm were assigned to the protons of conjugated triene in TO triglycerides. However, the intensity of these peaks significantly decreased in the TOMA spectrum. Additionally, new peaks at 2.9-3.5 ppm appeared in the TOMA spectrum, corresponding to the protons on the connecting sites between TO and MA. In the TMH spectrum, the peaks in the range of 5.6-6.2 ppm were attributed to the introduced C=C protons from TBEM.

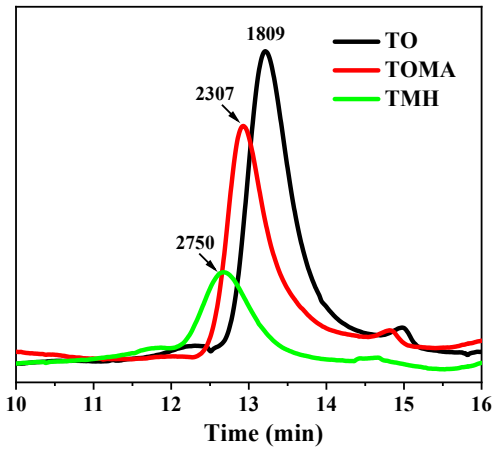

Fig. S19. GPC spectra of TO, TOMA, and TMH.

Table S1. The number-average molecular and weights weight-average of TO, TOMA, and TMH.

Samples	M_n	M_w	M_w/M_n
TO	1566	1769	1.13
TOMA	2029	2131	1.05
TMH	2708	3067	1.13

Both products TOMA and TMH exhibited only a narrow and single peak, indicating that the synthesized products are relatively homogeneous with minimal occurrence of self-polymerization. The M_w and M_n values of TMH were significantly higher at 3067 and 2708 g/mol, respectively, compared to TOMA (M_w = 2131, M_n = 2029).

3.9. Compositions for the UV-cured TMHA samples.

Table S2. Compositions for the UV-cured TMHA samples.

Samples	TMH (wt %)	HEA (wt %)	Darocur 1173 (wt %)
TMHA1	90	10	2
TMHA2	80	20	2
TMHA3	70	30	2
TMHA4	60	40	2

3.10. Scratch-repairing curves of the TMHA2 sample at different temperatures and times

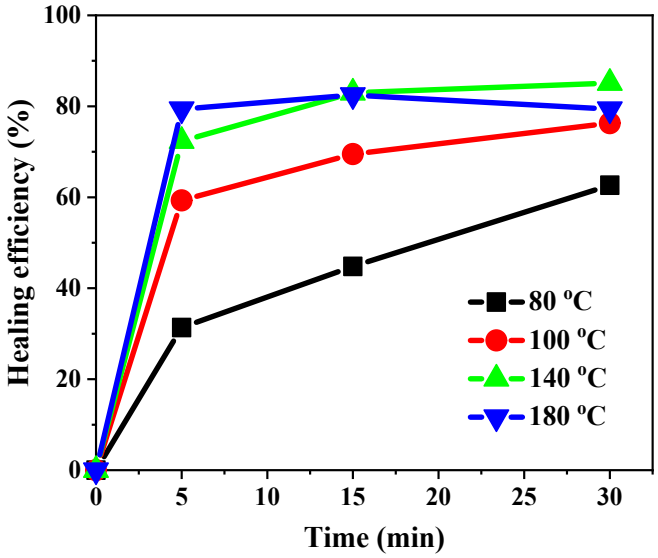

Fig. S20. Scratch-repairing curves of the TMHA2 sample at different temperatures and times.

3.11. Mechanical properties of TMHA2 after recycling

Table S3. Mechanical properties of TMHA2 after recycling.

Samples	σ (MPa)	R_e * (%)	ε (%)	R_e * (%)	E (MPa)	R_e * (%)
TMHA2	14.8 ± 2.2	-	80.9 ± 11.3	-	233.2 ± 19.7	-
Cycle 1	15.1 ± 2.4	102.0	70.9 ± 18.2	102.7	239.6 ± 27.9	87.6
Cycle 2	12.0 ± 1.8	81.1	60.3 ± 11.6	81.3	189.7 ± 31.2	74.5
Cycle 3	10.0 ± 0.7	67.6	54.1 ± 7.9	44.6	103.9 ± 24.6	66.9

* Recycling efficiency for each kind of property.

References

1. J. Zhang, Q. Shang, Y. Hu, F. Zhang, J. Huang, J. Lu, J. Cheng, C. Liu, L. Hu, H. Miao, Y. Chen, T. Huang and Y. Zhou, *Eur. Polym. J.*, 2020, **140**, 109997.
2. C. Zhang, H. Liang, D. Liang, Z. Lin, Q. Chen, P. Feng and Q. Wang, *Angew. Chem. Int. Ed. Engl.*, 2020, **60**, 4289-4299.
3. W.-Q. Yuan, G.-L. Liu, C. Huang, Y.-D. Li and J.-B. Zeng, *Macromolecules*, 2020, **53**, 9847-9858.
4. A. Barth, *Prog. Biophys. Mol. Biol.*, 2000, **74**, 141–173.
5. Z. Yu, S. Ma, Z. Tang, Y. Liu, X. Xu, Q. Li, K. Zhang, B. Wang, S. Wang and J. Zhu, *Green Chem.*, 2021, **23**, 6566-6575.